

# Elastic geobarometry for anisotropic inclusions in cubic hosts

M.L. Mazzucchelli<sup>a,\*</sup>, A. Reali<sup>b</sup>, S. Morganti<sup>c</sup>, R.J. Angel<sup>a,d</sup>, M. Alvaro<sup>a</sup>

<sup>a</sup> Department of Earth and Environmental Sciences, University of Pavia, Via Ferrata 1, 27100, Pavia, Italy

<sup>b</sup> Department of Civil Engineering and Architecture, University of Pavia, 27100, Pavia, Italy

<sup>c</sup> Department of Electrical, Computer and Biomedical Engineering, University of Pavia, 27100, Pavia, Italy

<sup>d</sup> Istituto di Geoscienze e Georisorse, CNR, Via Giovanni Gradenigo 6, 35131, Padova, Italy

## ARTICLE INFO

### Article history:

Received 17 May 2019

Received in revised form

9 September 2019

Accepted 14 September 2019

Available online 8 October 2019

### Keywords:

Elastic geobarometry

Elastic anisotropy

Elastic relaxation

Host-inclusion systems

Finite element method

## ABSTRACT

Mineral inclusions entrapped in other minerals may record the local stresses at the moment of their entrapment in the deep Earth. When rocks are exhumed to the surface of the Earth, residual stresses and strains may still be preserved in the inclusion. If measured and interpreted correctly through elastic geobarometry, they give us invaluable information on the pressures ( $P$ ) and temperatures ( $T$ ) of metamorphism. Current estimates of  $P$  and  $T$  of entrapment rely on simplified models that assumes that the inclusion is spherical and embedded in an infinite host, and that their elastic properties are isotropic. We report a new method for elastic geobarometry for anisotropic inclusions in quasi-isotropic hosts. The change of strain in the inclusion is modelled with the axial equations of state of the host and the inclusion. Their elastic interaction is accounted for by introducing a 4<sup>th</sup> rank tensor, the relaxation tensor, that can be evaluated numerically for any symmetry of the host and the inclusion and for any geometry of the system. This approach can be used to predict the residual strain/stress state developed in an inclusion after exhumation from known entrapment conditions, or to estimate the entrapment conditions from the residual strain measured in real inclusions. In general, anisotropic strain and stress states are developed in non-cubic mineral inclusions such as quartz and zircon, with deviatoric stresses typically limited to few kbars. For garnet hosts, the effect of the mutual crystallographic orientation between the host and the inclusion on the residual strain and stress is negligible when the inclusion is spherical and isolated. Assuming external hydrostatic conditions, our results suggest that the isotropic and the new anisotropic models give estimations of entrapment conditions within 2%.

© 2019 The Author(s). Published by Elsevier B.V. This is an open access article under the CC BY license (<http://creativecommons.org/licenses/by/4.0/>).

## 1. Introduction

After entrapment, mineral inclusions can develop residual strains and stresses as a result of the contrast in elastic properties with their hosts. If the elastic strains and stresses are preserved after entrapment and exhumation to room conditions, they can be used to estimate the entrapment conditions using elastic geobarometry. Several studies have reported examples of successful application of elastic geobarometry (e.g., Enami et al., 2007; Thomas and Spear, 2018). However, some discrepancies still exist that pose limitations to the applicability of the current methodologies mostly because the available models (e.g., Zhang, 1998; Guiraud and Powell, 2006; Angel et al., 2017b) are based on a simplified geometry of the system (with a spherical inclusion sitting in an infinite host) and the use of isotropic elastic properties

for both the host and the inclusion. Mazzucchelli et al. (2018) showed how to apply elastic geobarometry to systems with non-ideal geometry, but still with the assumption that both the host and the inclusion are elastically isotropic. However, no mineral is elastically isotropic and the anisotropy might significantly affect the results of elastic geobarometry even for a simple spherical inclusion (e.g., Zhang, 1998; Burnley and Schmidt, 2006; Angel et al., 2014; Campomenosi et al., 2018). Here, we present a new solution for elastic geobarometry that includes the elastic anisotropy of the mineral pair assuming that the geometry of the system is ideal, with a spherical inclusion embedded in an effectively infinite host. We show that deviatoric strain and stress fields are developed during exhumation in inclusions with crystallographic symmetry lower than cubic. For garnet hosts and assuming a simple geometry of the system, the new anisotropic model and the isotropic model predict similar residual values of the volume strain developed in the inclusion after exhumation, that are usually within the typical uncertainties on the measurements of the strain in natural inclusions. As a consequence, the back-calculation of the entrapment

\* Corresponding author.

E-mail address: [mattialuca.mazzucchelli@unipv.it](mailto:mattialuca.mazzucchelli@unipv.it) (M.L. Mazzucchelli).

conditions with the isotropic and the anisotropic models gives results within 2%. Extensions of this analysis to the real geometries of natural samples are also discussed.

## 2. Background

When the host mineral is elastically isotropic, it will expand isotropically upon exhumation and recovery to room conditions. A spherical inclusion within the host will therefore be forced to change in size but will always remain spherical (Fig. 1). It is therefore subject to an isotropic strain. If the inclusion is isotropic it will have isotropic compressibility and it will therefore exhibit isotropic stress equal in all directions; the normal stresses in any three perpendicular directions will be equal, and the inclusion will be subject to a hydrostatic pressure. The final pressure in the inclusion at any external pressure ( $P$ ) and temperature ( $T$ ) applied to the host can be calculated in two steps. The first is the calculation of the volume change of the host due to the change in  $P$  and  $T$ . This volume change is then applied to the inclusion, resulting in a pressure  $P_{thermo}$  that is purely the consequence of the contrast in the Equations of State (EoS) of the two minerals. For most  $P$  and  $T$  changes, the inclusion will exhibit a  $P_{inc}$  that is different from the external pressure on the host. This pressure difference drives a mutual elastic relaxation that always decreases the contrast between the  $P_{inc}$  and the external pressure. The calculation of the pressure change due to relaxation is the second step in any calculation of the final inclusion pressure.

When both the inclusion and the host mineral are isotropic, the calculation of the residual pressure in the inclusion relies on the concept of entrapment isomeke of the two minerals (Angel et al., 2015b, 2014b). Along an entrapment isomeke the pressure in an isotropic inclusion remains equal to the external pressure on the host, and the stress field inside the inclusion is homogeneous and isotropic. This uniform stress state is critical to the calculation of the relaxation for isotropic systems with spherical symmetry (Angel et al., 2017b, 2014b). For spherical systems the pressure change in the inclusion due to the relaxation ( $\Delta P_{relax}$ ) can be calculated from the change in volume of the host during exhumation and the non-

linear variation of the bulk modulus of the inclusion with pressure (its equation of state). The  $\Delta P_{relax}$  can also be calculated from a measured final  $P_{inc}$  and used to back-calculate possible conditions of entrapment of an inclusion. For non-spherical systems the amount of relaxation is also function of the overall geometry of the system, i.e. the shape of the inclusion and its position within the host (Mazzucchelli et al., 2018).

However, minerals are always elastically anisotropic. Cubic minerals are a special class. They are elastically anisotropic because their elastic stiffness (which depends on the 4<sup>th</sup> rank elasticity tensors, Nye, 1985) varies with direction, with the two extreme values along the  $\langle 111 \rangle$  and  $\langle 100 \rangle$  families of directions (Nye, 1985). However, the response of a crystal to hydrostatic stress is governed by the 2<sup>nd</sup> rank compressibility tensor, which is isotropic for cubic crystals (e.g Angel et al., 2009; Nye, 1985). Therefore, due to their high crystallographic symmetry, under hydrostatic stress cubic crystals will always develop isotropic strain, similarly to isotropic materials. Therefore, a cubic host will impose an isotropic strain on the inclusion if the external conditions are hydrostatic. But if the inclusion has a symmetry lower than cubic, the imposed isotropic strain field must generate an anisotropic stress field, in which the stresses are different in different directions. The development of anisotropic stresses in inclusions can also be understood by a thought experiment (Fig. 1). Consider a spherical inclusion crystal trapped in a spherical cavity within the host at the  $P$  and  $T$  conditions of entrapment. For simplicity we consider the case of the inclusion being softer than the host. Now remove the inclusion crystal from the host and bring both the host and inclusion crystals to room conditions. Both crystals will expand according to the normal behaviour of free crystals under hydrostatic pressure, with the inclusion expanding more than the cavity of the host. If both crystals are elastically isotropic or cubic, then both the cavity in the host and the inclusion crystal remain spherical, and an isotropic stress (i.e. a hydrostatic pressure) is required to force the crystal back into the cavity (Fig. 1a). The inclusion must therefore be under a hydrostatic stress in this case. If the inclusion is anisotropic it will expand more in some directions than others so that it will become an ellipsoid at room pressure (Fig. 1a). It is clear that an anisotropic

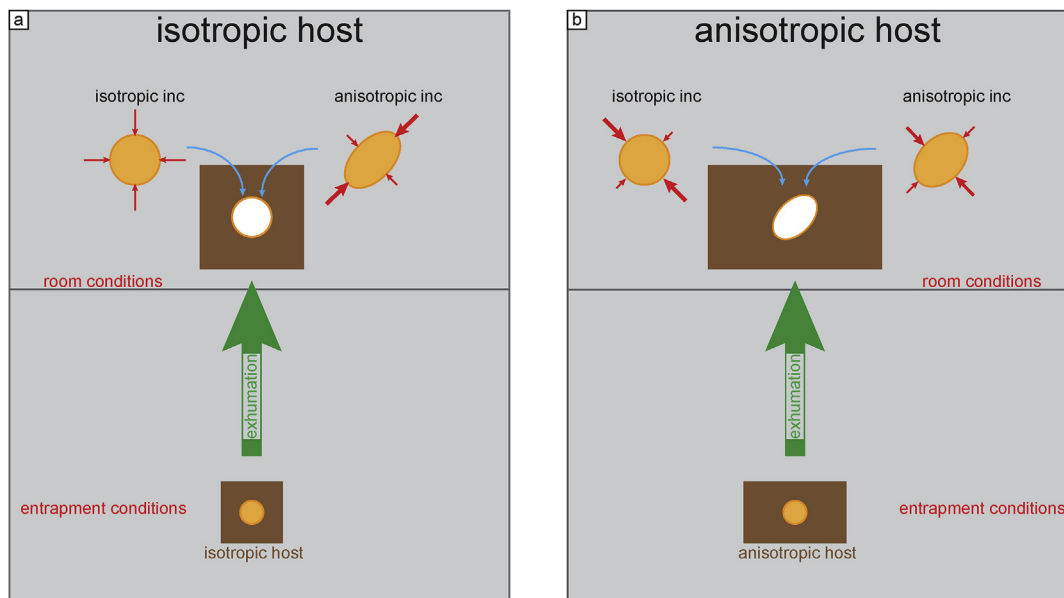


**Fig. 1.** Exhumation of the host from entrapment to room conditions: (a) if the host is isotropic or cubic the spherical cavity remains spherical after exhumation. The stress required to force an inclusion crystal into the cavity is isotropic if the inclusion is elastically isotropic, but an anisotropic stress is required for an anisotropic inclusion. (b) If the host is elastically anisotropic the shape of the cavity changes upon exhumation. In this case, the stress required to push the inclusion back into the cavity is anisotropic, even when the inclusion is elastically isotropic.

stress is required to force the inclusion to fit back into the cavity of a cubic host, and these anisotropic stresses will therefore be present in the trapped inclusion recovered to room conditions. For an anisotropic host, an isotropic inclusion crystal will remain spherical when recovered to room conditions but requires anisotropic stress to force it into the ellipsoidal cavity developed on exhumation of an anisotropic host (Fig. 1b). When both phases are non-cubic the non-hydrostatic stress required (Fig. 1b) depends on the mutual crystallographic orientation of the host and inclusion crystals.

Minerals with symmetry less than cubic develop deviatoric stresses when an isotropic strain is applied to them. Therefore, if at least one of the host and the inclusion is not cubic, the entrapment isomeke is no longer a valid basis for calculating the relaxation, even for spherical inclusions, because the stress in the inclusion does not remain isotropic and therefore it cannot be equal to the hydrostatic pressure in the host. Instead, we introduce a thermodynamic calculation that considers explicitly the variation in length of the axes of the inclusion imposed by the change in size of the host cavity during the exhumation from entrapment to room conditions. The resulting strain in the inclusion is then relaxed to find the final stress and strain in the inclusion. In this case the anisotropic relaxation can only be calculated using numerical simulations following the procedure developed and described in this paper.

### 3. Methods

#### 3.1. Extension to elastic anisotropy

The extension of elastic geobarometry to include elastic anisotropy is best illustrated with the forward-calculation from the entrapment conditions ( $P_{trap}$ ,  $T_{trap}$ ) to the final residual strain and stress developed in the inclusion after the exhumation to the Earth's surface. As for the case of isotropic geobarometry, this calculation is split into two steps: thermodynamic calculation and relaxation.

Instead of using the entrapment isomeke as a basis for the calculation of relaxation (Angel et al., 2014b) we use the thermodynamic calculation. For isotropic minerals, when the host is at the final external pressure and temperature  $P_{end}$  and  $T_{end}$ , the inclusion is constrained to the volume of the cavity within the host at these conditions. We will call this cavity volume  $V_{host}(P_{end}, T_{end})$ . The pressure  $P_{thermo}$  in the inclusion is determined by the EoS of the inclusion and this volume at the final temperature  $T_{end}$ . Under these conditions the volume change of the cavity in the host from entrapment to the final conditions is the same as the inclusion from entrapment to  $P_{thermo}$ , which can be expressed as:

$$\frac{V_{host}(P_{trap}, T_{trap})}{V_{host}(P_{end}, T_{end})} = \frac{V_{inc}(P_{trap}, T_{trap})}{V_{inc}(P_{thermo}, T_{end})} \quad (1)$$

Because we have only one constraint on the state of the inclusion, its pressure  $P_{inc}$  or equivalently its volume strain, we are not able to define a unique  $P$  and  $T$  of entrapment, but only a line in the  $P$ - $T$  space.

Eq. (1) shows that entrapment conditions are also defined as states where there are no strain gradients across the host and inclusion, and this insight allows a new approach to be developed for other cases. For isotropic and cubic materials, the cube-root of the volume change is equal to the change in linear dimensions, so Eq. (1) can also be written as:

$$\left[ \frac{V_{host}(P_{trap}, T_{trap})}{V_{host}(P_{end}, T_{end})} \right]^{1/3} = \left[ \frac{V_{inc}(P_{trap}, T_{trap})}{V_{inc}(P_{thermo}, T_{end})} \right]^{1/3} \quad (2)$$

This emphasises that the conditions for entrapment are that the

linear dimensions of the free host and inclusion crystals must be equal at the time of entrapment in order to not have stress or strain gradients across the system. If the inclusion phase is non-cubic, we can write for any crystallographic direction of length  $l_i$  (with  $i = 1, 2, 3$ ) that the entrapment conditions in a cubic host mineral are defined by:

$$\left[ \frac{V_{host}(P_{trap}, T_{trap})}{V_{host}(P_{end}, T_{end})} \right]^{1/3} = \frac{l_{i,inc}(P_{trap}, T_{trap})}{l_{i,inc}(P_{thermo}, T_{end})} \quad (3)$$

For a uniaxial inclusion (e.g. quartz and zircon), if the variation of unit-cell parameters of the inclusion with  $P$  and  $T$  are known, then each of the  $a$  and  $c$  axes allows a line of possible entrapment conditions to be calculated from Eq. (3). The intersection of these two lines provides a unique  $P$  and  $T$  of entrapment. For a biaxial inclusion (e.g., orthorhombic crystals), three independent lines can be calculated. If the three lines do not intersect at a single point within the uncertainties, this would be a signal of deviatoric stresses being present at the time of entrapment. The same principle expressed in Eq. (3) can be applied to non-cubic inclusions trapped in non-cubic hosts by replacing the left-hand side with the lattice spacing of the direction in the host parallel to  $l_{i,inc}$ .

Eq. (3) can be rearranged to refer the change in length of each crystallographic direction of the inclusion during exhumation to the length  $l_{i,inc}(P_{end}, T_{end})$  it would have as a free crystal at the final  $P_{end}$ ,  $T_{end}$  of the host:

$$\left[ \frac{V_{host}(P_{end}, T_{end})}{V_{host}(P_{trap}, T_{trap})} \right]^{1/3} = \frac{l_{i,inc}(P_{thermo}, T_{end})}{l_{i,inc}(P_{end}, T_{end})} \frac{l_{i,inc}(P_{end}, T_{end})}{l_{i,inc}(P_{trap}, T_{trap})} \quad (4)$$

Using Voigt's notation (Voigt, 1910), in which the strain tensor can be represented as a vector, the normal strains imposed by a cubic host on the inclusion are:

$$\begin{aligned} \varepsilon_i^{unrel} &= \frac{l_{i,inc}(P_{thermo}, T_{end})}{l_{i,inc}(P_{end}, T_{end})} - 1 \\ &= \left[ \frac{V_{host}(P_{end}, T_{end})}{V_{host}(P_{trap}, T_{trap})} \right]^{1/3} \frac{l_{i,inc}(P_{trap}, T_{trap})}{l_{i,inc}(P_{end}, T_{end})} - 1 \end{aligned} \quad (5)$$

where  $\varepsilon_i^{unrel}$  is the unrelaxed strain relative to a free crystal calculated along the  $i$ -th direction of the inclusion. As shown by Eq. (5) the unrelaxed strain can be calculated if the variation with  $P$  and  $T$  of the volume of the host (i.e. its volume EoS) and of the axes of the inclusion (i.e. the 'axial' EoS, e.g., Angel et al., 2014a) are known. This state of strain corresponds to a stress field in the inclusion that is in general anisotropic and different to the stress state in the host (that is at room  $P$ ). Therefore, the stresses in the inclusion are not balanced out in the host, and this forces the relaxation of the system until mechanical equilibrium is reached again. When one or both of the host and the inclusion are elastically anisotropic, the relaxation (even for a spherical inclusion) is different in each direction. The amount of relaxation along a given direction depends on the full state of stress in the inclusion, the full anisotropic elastic properties, and the mutual crystallographic orientation of the pair. To a first approximation, the amount of relaxation along a specific direction in the inclusion is a consequence of both the stiffness of the host and of the inclusion along that direction. If the inclusion and the host both have cubic symmetry the relaxation is equal along each of the crystallographic axes of the inclusion. If the inclusion has a symmetry lower than cubic and the host is cubic, the largest relaxation is along the stiffest direction of the inclusion. However, the relaxation is a force-balance process and, as a consequence, more stressed directions tend to relax more.

Therefore, the amount of elastic relaxation depends on the overall balance between the stiffnesses of the host and of the inclusion and the magnitude of the unrelaxed stress along each direction.

The problem of calculating the variation of the stress and strain fields due to the relaxation is related to Eshelby's equivalent inclusion problem, that provides an analytical solution for the strain in an ellipsoidal inclusion embedded in an infinite isotropic host through the application of the so-called Eshelby's tensor (Eshelby, 1957). This solution was extended to other specific crystallographic symmetries (e.g., transversely isotropic symmetry, Chiang, 2017), but not to those typical of minerals from high-pressure metamorphic rocks (e.g., garnets, zircon), nor to faceted inclusion shapes. For the latter, the change in strain upon relaxation must be found with numerical calculations such as finite element analysis (Hughes, 2012). This approach does not introduce any restriction given by the elastic anisotropic properties of the host and of the inclusion and their reciprocal orientation. However, the entire procedure would be time consuming and would greatly restrict the routine applicability of elastic geobarometry because a new finite element analysis is in principle required for any specific initial unrelaxed strain state. This can be avoided by assuming that the elastic properties of both the host and the inclusion remain constant during the relaxation. Under this assumption, we can introduce a fourth order non-symmetric tensor (the relaxation tensor  $R_{ijkl}$ ) to transform the unrelaxed strain into the relaxed strain, and vice versa. Once the relaxation tensor is calculated for a specific geometry and mutual orientation it can be applied to relax any unrelaxed strain state for that system, with no need for further finite element analyses.

### 3.2. The relaxation tensor ( $R$ )

Adopting Voigt's notation (i.e. expressing the strain as a six-component vector), to express the relaxation we look for a linear mapping  $f: R^6 \mapsto R^6$  that relates the relaxed and the unrelaxed strain,  $f(\epsilon_j^{\text{unrel}}) = \epsilon_j^{\text{rel}}$ . This linear mapping can be defined through a matrix  $\mathbf{R} \in R^{6 \times 6}$ . The columns of  $\mathbf{R}$  are found from the response, computed by means of finite element analysis, to six predefined strain states, each characterized by only one non-zero component. The matrix  $R_{ij}$ , that has 6 columns and 6 rows, is the representation in Voigt notation of the relaxation tensor  $R_{ijkl}$  which is a 4<sup>th</sup> rank tensor because it relates two 2<sup>nd</sup> rank tensors (the tensors of the relaxed and unrelaxed strain). The  $R_{ijkl}$  tensor does not possess the major symmetries and can have up to 36 independent components, and, as consequence, the  $R_{ij}$  matrix also has up to 36 non-zero components and is non-symmetric. The components of  $\mathbf{R}$  depend on the elastic properties of the host and the inclusion and the geometry of the system (e.g. the shape of the inclusion). Moreover, if both the inclusion and the host are elastically anisotropic, the components of the relaxation tensor will depend upon the mutual crystallographic orientation of the host and the inclusion and must be recalculated for each orientation. Therefore, in general, a relaxation tensor is applicable only to systems with the specific geometry and mutual orientation for which it was calculated. It can be applied to calculate the relaxed strain in the inclusion from the unrelaxed strain (obtained from Eq. (5)) and vice versa. In Voigt notation:

$$\begin{aligned} \epsilon_i^{\text{rel}} &= R_{ij} \epsilon_j^{\text{unrel}} \\ \epsilon_i^{\text{unrel}} &= R_{ij}^{-1} \epsilon_j^{\text{rel}} \end{aligned} \quad (6)$$

The  $\mathbf{R}$  tensor is calculated under the assumption of linear elasticity (small strains and constant elastic properties), which is not true in general for geological materials. However, this is a good

approximation for inclusions since  $\mathbf{R}$  is only applied to compute small changes in strain during the relaxation at room temperature which correspond to stress variations typically much smaller than 1 GPa. Moreover,  $\mathbf{R}$  depends on the difference in the elastic moduli of the host and the inclusion which, for minerals, have a similar dependence on pressure. Furthermore, the estimated errors in the change of the strain during relaxation are smaller than those arising from the combined uncertainties on the measured strains and those on the elastic tensor coefficients, which amount to about 1%. The advantage of this approach is that the  $\mathbf{R}$  tensor then becomes independent of the magnitude of the residual strains. Once the  $\mathbf{R}$  tensor has been calculated for a specific host-inclusion system, it can be used for any inclusion and host with the same properties, geometry and orientation. Further details about the definition and the derivation of the relaxation tensor are reported in the supplementary data.

The relaxation tensor can be only applied to relax the strain in the inclusion, and not directly to the stress. The final stress in the inclusion must be calculated from the strain using the elastic stiffness tensor (written in Voigt notation as a matrix,  $C_{ij}^{\text{inc}}$ ) of the inclusion:

$$\sigma_i^{\text{rel}} = C_{ij}^{\text{inc}} \epsilon_j^{\text{rel}} = C_{ij}^{\text{inc}} \left( R_{jk} \epsilon_k^{\text{unrel}} \right) \quad (7)$$

However, the inclusion is not at room  $P$  but usually under a deviatoric stress field, and the components of the stiffness tensor vary as a function of the stress state. Unfortunately, the stress dependency of the  $C_{ij}$  of minerals is not yet known and it cannot be directly inferred from their pressure dependency measured experimentally (e.g. Wang et al., 2015). For stiff minerals, such as diamond or garnets, the  $C_{ij}$  values do not vary much with the small stress variation due to the elastic relaxation and the use of room pressure elastic properties leads to very small uncertainties on the final stress components calculated with Eq. (7). However, uncertainties become larger for soft materials such as quartz, whose elastic properties change rapidly with pressure (Wang et al., 2015).

We have calculated the  $\mathbf{R}$  tensor for a number of cases, varying the contrast in stiffness between the host and the inclusion but keeping a simple geometry of the system (i.e. a spherical inclusion in a practically infinite host). This allows us to show in the following section the calculation of the final strain and stress developed during the exhumation of several host-inclusion systems typical of ultra-high pressure metamorphic rocks.

## 4. Examples

In our examples we use aluminosilicate garnets (e.g., pyrope and grossular) as hosts and diamond, quartz and zircon as inclusions. This choice of pairs allows us to focus on how the anisotropy and the stiffness of the inclusion affects the calculation. Garnets are highly resistant to viscous relaxation (e.g. Karato et al., 1995; Zhong et al., 2018) even at high  $P$  and  $T$  metamorphic conditions. This enables us to calculate the final strain and stress in the inclusion as a function of the entrapment conditions within the elastic limit for most cases. For each host-inclusion system we defined a grid of entrapment conditions. For each initial point of entrapment, we combined the thermodynamic calculation and the elastic relaxation to compute the strain and the stress developed in the inclusion during the exhumation and the difference between the true volume strain obtained from the anisotropic model and that calculated with the isotropic solution (Angel et al., 2017b). Moreover, by comparing the two models we also show the magnitude of the errors in the calculation of the entrapment pressure if one assumes that minerals are isotropic. The EoS for pyrope and grossular used for the thermodynamic part of the anisotropic calculation and for the isotropic calculation are from Milani et al. (2017, 2015). The

stiffness tensors for the calculation of the relaxation tensor are from Sinogeikin and Bass (2002) and Isaak et al. (1992) respectively (further details in the supplementary data).

In general, when both the host and the inclusion are elastically anisotropic the strain and the stress calculated in the inclusion are also a function of the relative crystallographic orientation between the two crystals. However, since garnets are cubic, the relative orientation between the host and the inclusion does not affect the thermodynamic calculations. If the initial (entrapment) and final ( $P_{room}$ ,  $T_{room}$ ) conditions are under external lithostatic stress, a cubic host will develop an isotropic strain field. Therefore, an inclusion with symmetry less than cubic, that is forced to deform as the cavity in the host, will develop an anisotropic stress field which is not affected by its relative orientation within the host. However, when the elastic interaction between the host and the inclusion is computed (i.e. the relaxation step) their mutual orientation becomes relevant, because the stiffness of minerals (even cubic minerals, see discussion above) varies with the direction. For example, if the stiffest direction of the inclusion points toward the softest direction of the host the relaxation along that direction will be maximized. Therefore, the final residual strain in the inclusion is also function of the mutual crystallographic orientation between the host and the inclusion and the components of the relaxation tensor must be recomputed for each orientation. However, we show that for garnet hosts, that are almost isotropic, the relative orientation of a spherical inclusion introduces deviations in the residual strain that are negligible when compared to the uncertainties in the measurements on natural samples. To prove this concept, for each inclusion-garnet pair we investigated two representative orientations, aligning the stiffest direction of the inclusion with the stiffest and softest directions of the host respectively (more details in the supplementary data).

#### 4.1. Cubic inclusion in cubic host: diamond in garnet

We show the results for a spherical inclusion of diamond with its [1 1 1] direction aligned with the [1 1 1] direction of the garnet (i.e. pyrope and grossular) host. The EoS and the stiffness tensor of diamond are from Angel et al. (2015) and Zouboulis et al. (1998), respectively. We follow the usual convention for which the strain and the stress are defined in a Cartesian reference system for which the normal components of the strain and of the stress are parallel to

the  $\langle 1\ 0\ 0 \rangle$  crystallographic directions.

After the thermodynamic calculation from entrapment to the final temperature ( $T_{end}$ ), a cubic inclusion in a cubic host is subject to isotropic strain and stress and, as a result, the strain (and the stress since the crystal is cubic) are isotropic before relaxation (see Eq. (2)). This together with the symmetry of the top left block of the  $\mathbf{R}$  tensor (i.e.  $R_{11} = R_{22} = R_{33}$ ,  $R_{12} = R_{13} = R_{23}$ , see Table S2.4) guarantees that the final strain in the inclusion after exhumation is isotropic for any entrapment  $P$  and  $T$ . We calculated the volume strain developed in the inclusion after exhumation from a wide range of entrapment  $P_{trap}$ ,  $T_{trap}$  to room conditions. Fig. 2 shows that the final inclusion volume strain calculated with the anisotropic model ( $\epsilon_V^{aniso} = \epsilon_1 + \epsilon_2 + \epsilon_3$ ) is practically equal to the result of the isotropic model ( $\epsilon_V^{iso}$ ). The small deviation is due to the non-linear elasticity used for the isotropic relaxation and to the elastic anisotropy of the host and the inclusion. Since cubic minerals are not elastically isotropic, their Reuss ( $G_R$ ) and Voigt ( $G_V$ ) shear moduli are not equal as they would be in an isotropic material, leading therefore to a different elastic relaxation. From our calculation it is evident that the difference  $\epsilon_V^{iso} - \epsilon_V^{aniso}$  is slightly smaller for the grossular host that is stiffer than pyrope (compare Fig. 2 a and b). From a practical point of view, the isotropic model can be considered a good approximation if the difference in the final volume strain  $\epsilon_V^{iso} - \epsilon_V^{aniso}$  is smaller than the typical uncertainties associated with the measurements of the volume strain in natural inclusions. For diamond inclusions the residual strain ( $\epsilon_V$ ) can be determined by X-ray diffraction measurements with an uncertainty in the order of magnitude  $\delta(\epsilon_V) \approx 10^{-4}$  (Angel et al., 2016). As a consequence, Fig. 2 shows that the isotropic model gives the correct volume strain for both pyrope and grossular hosts, suggesting that for a diamond inclusion in garnet it may also be used to obtain a reliable estimation of the entrapment pressure. For example, for an entrapment at 4.2 GPa and 1000 °C, the final volume strain in the inclusion after the exhumation would be  $5.5 \cdot 10^{-4}$ . If that volume strain is measured (with X-ray diffraction or Raman spectroscopy) and used in an isotropic model, the recalculated entrapment pressure is  $P_{trap} = 4.15$  GPa (1% deviation from the true initial value). This result is particularly relevant when the measurement is performed with Raman spectroscopy, that for cubic minerals only gives the volume strain and therefore only allows the application of isotropic geobarometry (Angel et al., 2018). Moreover, Fig. S.2.2 (in supplementary data) shows that, despite the large contrast in

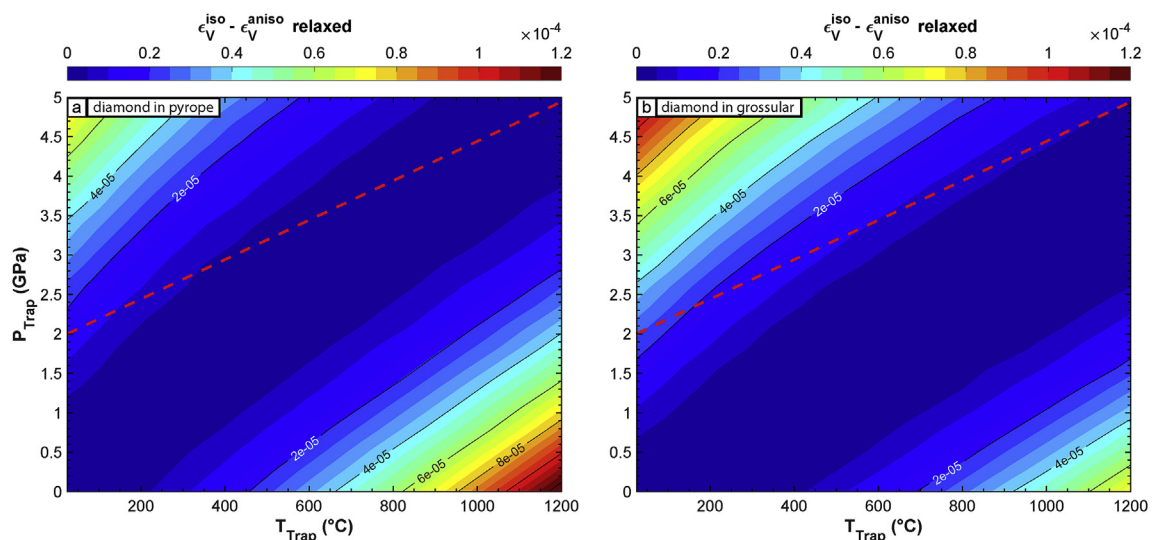


**Fig. 2.** Difference between the volume strain in the inclusion after exhumation from the  $P_{trap}$ ,  $T_{trap}$  of entrapment to room conditions calculated with the isotropic and the anisotropic models. (a) diamond in pyrope; (b) diamond in grossular. Dashed line is the graphite-diamond phase boundary from Day, 2012.

elastic properties between the diamond inclusion and the garnet host, their relative crystallographic orientation does not significantly affect the final volume strain in the inclusion. Therefore, the determination of their relative orientation is not necessary for the calculation of reliable entrapment conditions.

#### 4.2. Non-cubic inclusion in cubic host

##### 4.2.1. Quartz in garnet

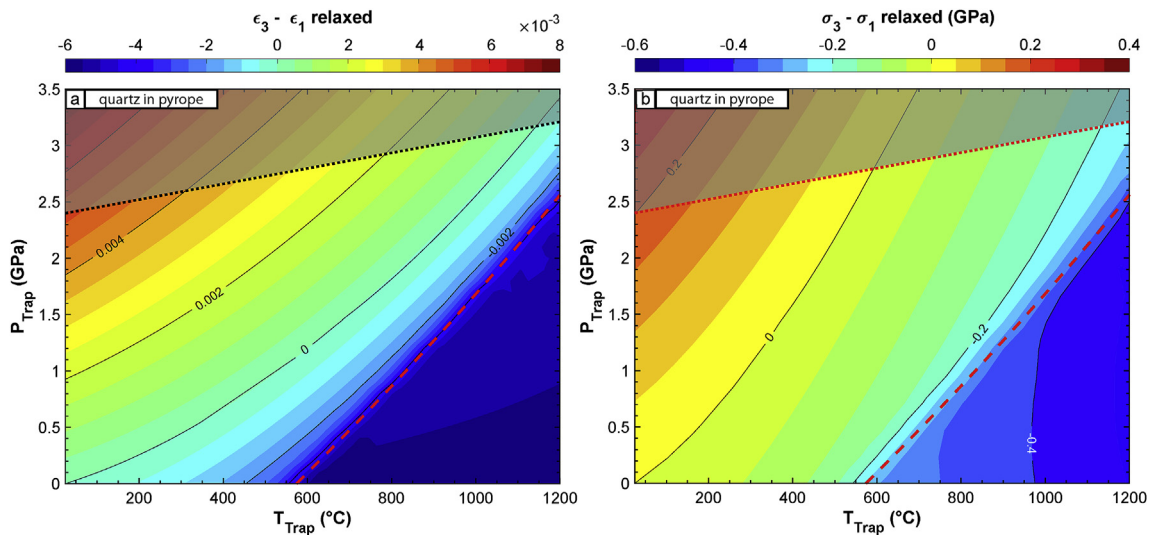
Here we report the results for a spherical quartz inclusion with its crystallographic  $c$ -axis aligned with the  $[0\ 0\ 1]$  direction of the garnet (i.e. pyrope and grossular) host. As shown by Eq. (5), the strain field developed during exhumation in a non-cubic inclusion in a cubic host is in general anisotropic, because quartz is uniaxial and the  $a$  and  $c$  crystallographic axes of the inclusion behave differently under changes of the external pressure and temperature. The EoS for quartz are from Angel et al. (2017a) and Alvaro et al., 2020 and explicitly include the effects of the  $\alpha$  -  $\beta$  transition in quartz. The stiffness tensor is from Lakshtanov et al. (2007). We again follow the usual convention for which the strain and the stress are defined in a Cartesian reference system for which the  $\epsilon_1$ ,  $\sigma_1$  and  $\epsilon_2$ ,  $\sigma_2$  components lie in the crystallographic  $a$ - $b$  plane and the  $\epsilon_3$ ,  $\sigma_3$  component is parallel to the  $c$ -axis.

Fig. 3a shows the differential strain  $\epsilon_3 - \epsilon_1$  calculated in the inclusion after exhumation from the  $P_{\text{trap}}$ ,  $T_{\text{trap}}$  of entrapment to room conditions. Since  $\epsilon_3$  is not necessarily the maximum strain in the inclusion, the difference  $\epsilon_3 - \epsilon_1$  can be either positive or negative depending on the entrapment conditions. The strain in the inclusion is isotropic only for a narrow range of entrapment conditions in  $P$ - $T$  space. Since quartz is trigonal, when the relaxed strain is isotropic the relaxed stress is not hydrostatic (see Fig. 3). When the strain is compressive (i.e. stresses are negative) and isotropic, the  $\sigma_3$  component of the stress is more negative than  $\sigma_1 = \sigma_2$  (because the quartz  $c$ -axis is stiffer than the  $a = b$  axes). As a consequence,  $\sigma_3 - \sigma_1$  is negative as can be seen by comparing Fig. 3a and b. On the other hand, when the compressive stress in quartz is isotropic the strain components  $\epsilon_1 = \epsilon_2$  are more negative than  $\epsilon_3$ , and  $\epsilon_3 - \epsilon_1$  is positive.

Fig. 4 shows that for entrapment at conditions in the  $\alpha$ -quartz

stability the true final volume strain in the inclusion obtained from the anisotropic model ( $\epsilon_V^{\text{aniso}}$ ) is more negative than the result of the isotropic model ( $\epsilon_V^{\text{iso}}$ ), and the difference  $\epsilon_V^{\text{iso}} - \epsilon_V^{\text{aniso}}$  is therefore positive. This difference is due to the use of the anisotropic elastic properties of the inclusion and to the assumption of constant elastic properties in the calculation of the anisotropic relaxation. The residual strain in natural quartz inclusions can be determined with Raman spectroscopy and X-ray diffraction (e.g. Murri et al., 2018). The uncertainty of the measurements of the Raman peak positions (evaluated as the reproducibility in multiple measurements of a standard reference crystal) is typically  $\approx 0.3\text{ cm}^{-1}$ . For quartz inclusions, by using the concept of phonon-mode Grüneisen tensors (Angel et al., 2018), this translates into an uncertainty on each component of the residual strain ( $\epsilon_i$ ) and on the volume strain ( $\epsilon_V$ ) of about  $10^{-3}$ . X-ray diffraction, has a better precision in the measurements and provide an uncertainties in the strains of about  $10^{-4}$ . Therefore, for a quartz inclusion in garnet the discrepancy between the isotropic and the anisotropic models would be smaller, or of the same order of magnitude, of the uncertainties in the experimental measurement of the volume strain. As a consequence, the isotropic model lead, to errors in the estimation of the entrapment pressure that are relatively small even at higher entrapment pressures, provided the true stress state of the inclusion is measured (Bonazzi et al., n.d.) For example, for an entrapment at 2.70 GPa and 800 °C, close to the quartz-coesite phase boundary, the final volume strain in the quartz after the exhumation would be  $-2.709 \cdot 10^{-2}$ . The entrapment pressure recalculated from this volume strain using the isotropic model is  $P_{\text{trap}} = 2.75\text{ GPa}$ , with a discrepancy of 2% (less than 0.5 kbar) from the true initial value.

Because quartz is trigonal, the orientation of the inclusion within the host could also affect the strain in the inclusion and increase the errors associated with the isotropic model. Fig. 5 shows the variation of the two independent components ( $\epsilon_1$  and  $\epsilon_3$ ) of the strain calculated with two extreme relative orientations of the quartz inclusion in pyrope (further details are given in the supplementary data). The component  $\epsilon_3$  of the strain changes more with orientation, because it is parallel to the  $c$ -axis that is the stiffest crystallographic axis in quartz. Fig. S2.5 and S2.6 (in



**Fig. 3.** Quartz in pyrope showing (a) differential strain and (b) differential stress in the inclusion after exhumation from the  $P_{\text{trap}}$ ,  $T_{\text{trap}}$  of entrapment to room conditions. Since quartz is trigonal, when the relaxed strain is isotropic the relaxed stress is not hydrostatic (compare a and b). The line of isotropic strain divides the  $P$ - $T$  space in two fields, one with  $\epsilon_3 - \epsilon_1 > 0$  at higher  $P_{\text{trap}}$  and the other with  $\epsilon_3 - \epsilon_1 < 0$  at lower  $P_{\text{trap}}$ . This is due to the  $c$ -axis of quartz having a lower compressibility and thermal expansion compared to the  $a$ - and  $b$ -axes (see elastic properties reported in the supplementary data). Dotted line is the quartz-coesite phase boundary (Bose and Ganguly, 1995), the dashed line is the  $\alpha$ - $\beta$  quartz phase boundary (Angel et al., 2017a). The quartz-coesite phase transition is not included in the thermodynamic calculation, and all the results calculated for  $P_{\text{trap}}$ ,  $T_{\text{trap}}$  conditions above the phase boundary do not represent the real behaviour of coesite.

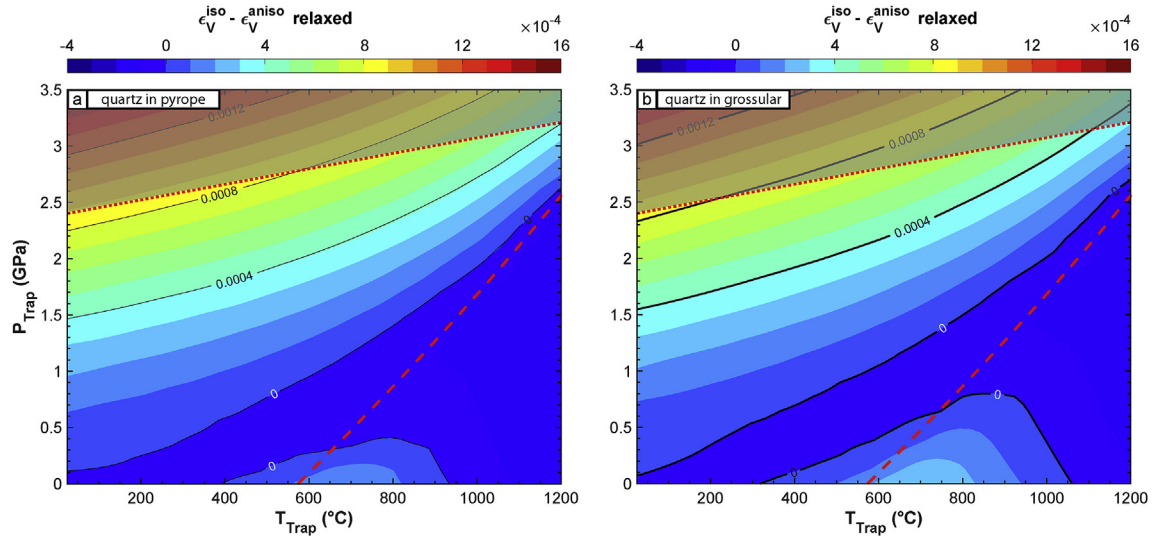


**Fig. 4.** Difference between the volume strain in the inclusion after exhumation from the  $P_{\text{Trap}}$ - $T_{\text{Trap}}$  of entrapment to room conditions calculated with the isotropic and the anisotropic models. (a) quartz in pyrope; (b) quartz in grossular. Dotted line is the quartz-coesite phase boundary (Bose and Ganguly, 1995), the dashed line is the  $\alpha$ - $\beta$  quartz phase boundary (Angel et al., 2017a). The quartz-coesite phase transition is not included in the thermodynamic calculation, and all the results calculated for  $P_{\text{Trap}}$ ,  $T_{\text{Trap}}$  conditions above the phase boundary do not represent the real behaviour of coesite.

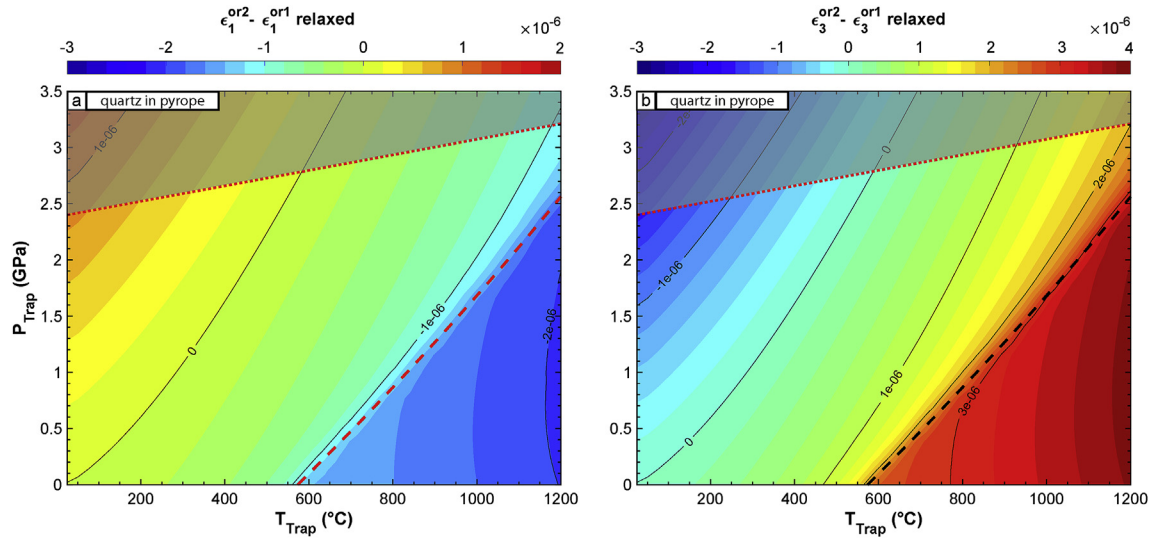


**Fig. 5.** Quartz in pyrope showing a comparison between the strain components  $\epsilon_1$  (a) and  $\epsilon_3$  (b) of the relaxed strain of the inclusion calculated for two different orientations: (or1)  $c$ -axis of quartz aligned with the stiffest direction (direction [001]) of pyrope; (or2)  $c$ -axis of quartz aligned with the softest direction (direction [111]) of pyrope. Dotted line is the quartz-coesite phase boundary (Bose and Ganguly, 1995), the dashed line is the  $\alpha$ - $\beta$  quartz phase boundary (Angel et al., 2017a). The quartz-coesite phase transition is not included in the thermodynamic calculation, and all the results calculated for  $P_{\text{Trap}}$ ,  $T_{\text{Trap}}$  conditions above the phase boundary do not represent the real behaviour of coesite.

supplementary data) show the change of the strain in the quartz inclusion taking grossular as host. Since grossular is slightly more anisotropic than pyrope the magnitude of the variation is slightly larger. However, for both pyrope and grossular hosts the change of the strain with orientation is very small and cannot be resolved with measurements such as X-ray diffraction or Raman spectroscopy that have an uncertainty on the determination of the strain components of  $\delta(\epsilon_i) \approx 1 \cdot 10^{-4}$ . Therefore, the relative orientation between the quartz inclusion and the garnet host does not significantly affect the strain in the inclusion.

#### 4.2.2. Zircon in garnet

Zircon, as quartz, is uniaxial and as a consequence the strain developed in a zircon inclusion during exhumation is in general anisotropic. Fig. 6 shows the strain developed after the exhumation

to room conditions in a spherical zircon inclusion with its crystallographic  $c$ -axis aligned with the [0 0 1] direction of the garnet (i.e. pyrope and grossular) host. The EoS and the stiffness tensor of zircon are from Zaffiro (2019) and Özkan et al. (1974), respectively. We continue to use the convention for which the strain and the stress are defined in a Cartesian reference system for which the  $\epsilon_1$ ,  $\sigma_1$  and  $\epsilon_2$ ,  $\sigma_2$  components lie in the crystallographic  $a$ - $b$  plane and the  $\epsilon_3$ ,  $\sigma_3$  component is parallel to the  $c$ -axis.

The final strain in the inclusion is perfectly isotropic only for an entrapment at low  $P$  and  $T$  conditions (Fig. 6). For any other entrapment  $P_{\text{Trap}}$ ,  $T_{\text{Trap}}$  the difference  $\epsilon_3 - \epsilon_1$  is always positive because the  $c$ -axis in zircon has a lower compressibility (is stiffer) than the  $a = b$  axes ( $\beta_{0,c} = 0.929 \cdot 10^{-3} \text{ GPa}^{-1}$ ,  $\beta_{0,a} = 1.69 \cdot 10^{-3} \text{ GPa}^{-1}$ ) but a larger thermal expansion ( $\alpha_{0,c} = 0.5095 \cdot 10^{-5} \text{ K}^{-1}$ ,  $\alpha_{0,a} = 0.2817 \cdot 10^{-5} \text{ K}^{-1}$ , Zaffiro, 2019). As expected, when the

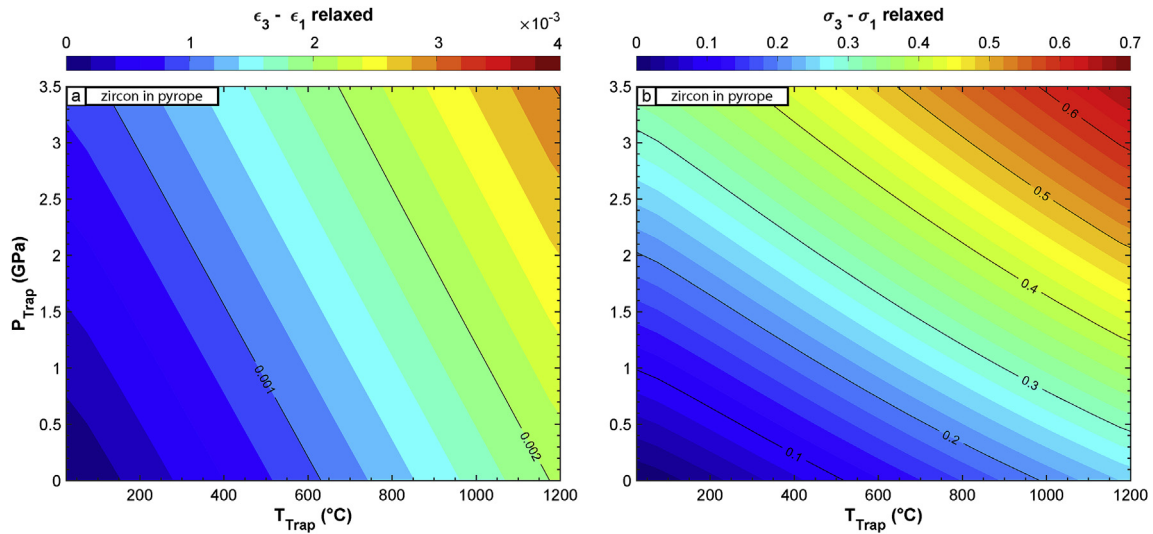


**Fig. 6.** Zircon in pyrope showing the (a) differential strain and (b) differential stress in the inclusion after exhumation from the  $P_{\text{Trap}}$ ,  $T_{\text{Trap}}$  of entrapment to room conditions.

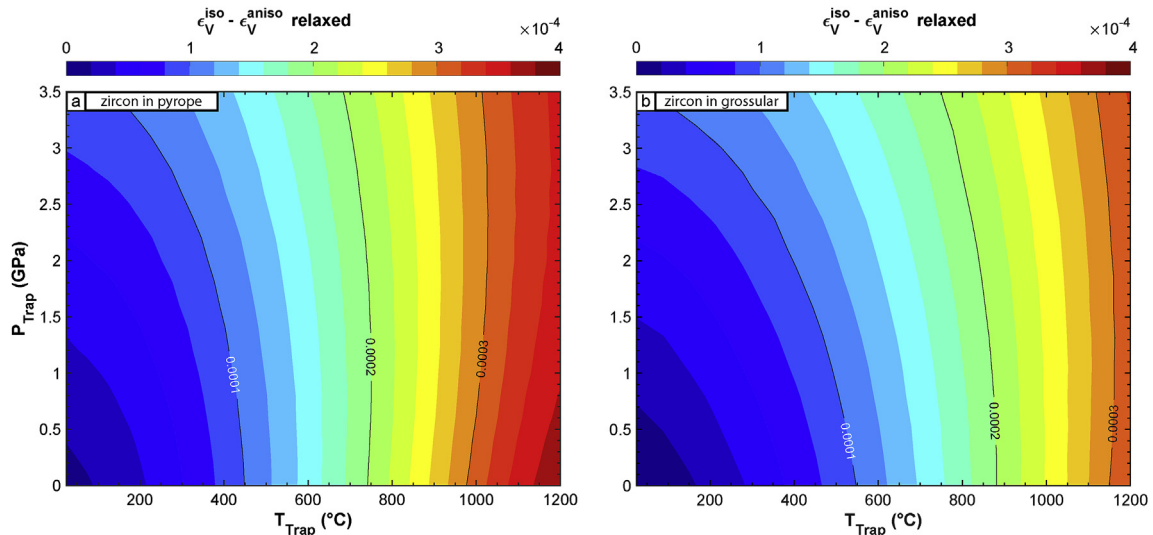


**Fig. 7.** Difference between the volume strain in the inclusion after exhumation from the  $P_{\text{Trap}}$ ,  $T_{\text{Trap}}$  of entrapment to room conditions calculated with the isotropic and the anisotropic models. (a) zircon in pyrope, (b) zircon in grossular.

differential strain is low (i.e. for entrapment at  $P_{\text{Trap}}$ ,  $T_{\text{Trap}}$  close to room conditions) the differential stress is also low (Fig. 6a and b). The stress, that is usually deviatoric, becomes hydrostatic only for entrapment at specific conditions which do not correspond to those that generate isotropic strain. The residual strain in a zircon inclusion can be measured by Raman spectroscopy or X-ray diffraction, that provide an uncertainty on the determination of the volume strain in the order of magnitude of  $10^{-4}$ . Fig. 7 shows that for all the entrapment conditions, and for both pyrope and grossular hosts, the discrepancy between the volume strain predicted by the isotropic and the anisotropic models is of the same order of magnitude of the uncertainties in the measurement of the volume strain.

The effect of the orientation of the zircon inclusion within the garnet host was tested for two extreme orientations (see supplementary data for further details). Fig. S2.7 - S2.10 (in supplementary data) show that for both pyrope and grossular hosts the relative orientation between the zircon inclusion and the host does not significantly affect the strain in the inclusion, since the change in strain could not be resolved with measurements that provide a

precision on the strains of  $\approx 10^{-4}$ . The variation of the strain due to the orientation is less for a pyrope host since it is elastically more isotropic than grossular.

## 5. Complex geometries

A detailed explanation for other geometries and host-inclusion pairs is beyond the scope of this paper. In general, the overall geometry of the system modifies the strain and stress developed in the inclusion during the exhumation. Therefore, the residual stress and strain fields in an inclusion with faceted morphology, or close to other inclusions or to the external surface of the host, may be different from the results shown in this work for an ideal geometry. As a consequence, for samples with non-ideal geometry the discrepancy in the calculation of the entrapment conditions between the anisotropic and the simple isotropic model might increase, if the geometrical features are not taken into account. However, the approach that we have outlined for simple spherical inclusions may be extended to more complex geometries. In this case precise constraints on the geometry of the system and on the

crystallographic orientations of the minerals can be obtained from X-ray micro-tomography and X-ray diffraction, respectively (e.g. Anzolini et al., 2019). Combining these pieces of information, a finite element model can be built to calculate the relaxation tensor that includes the effects of the shape of the inclusion, its proximity to external surfaces and to other inclusions, and its crystallographic orientation. An example of application for this procedure to a natural sample is reported in Alvaro et al., 2020. It should be remembered that the strain and stress fields, and, as consequence, the relaxation tensor are not constant in inclusions with non-elliptical shapes (Eshelby, 1957). Therefore, if the strain is measured in a specific point of the inclusion by Raman spectroscopy, the relaxation tensor should be calculated for that specific point from the finite element model on the real geometry. On the other hand, X-ray diffraction measurements give the average strain over the entire volume of the inclusion (e.g. Murri et al., 2018) and, in this case, an average relaxation tensor must be computed.

## 6. Conclusions

We have extended elastic geobarometry to include elastic anisotropy, by splitting the calculation of the final residual strain developed in the inclusion after exhumation into two steps: thermodynamic calculation and relaxation. With this approach the strain and the stress fields developed in the inclusion after the exhumation from any entrapment at external hydrostatic conditions can be computed.

Calculations confirm the expected result that when both the host and the inclusion have cubic crystallographic symmetry the residual strain and stress in the inclusion are always isotropic. If at least one of the host or the inclusion has a crystallographic symmetry lower than cubic, the relaxed strain and stress in the inclusion are generally anisotropic (and homogeneous if the inclusion is ellipsoidal), with differential stresses limited to few kilobars.

For garnet hosts and assuming a simple geometry of the system, the new anisotropic model and the isotropic model predict similar residual volume strains are developed in the inclusion after exhumation. The differences between the predictions of the isotropic and anisotropic calculations are usually within, or of the same order of magnitude of the typical uncertainties on the measurements of the strain in natural inclusions with X-ray diffraction or Raman spectroscopy. As we have shown, this implies that, for inclusions entrapped in cubic hosts at HP metamorphic conditions, the use of an elastically isotropic model for geobarometry leads to estimations of the entrapment pressure which are within 1 kbar of the results of the new anisotropic model. This is particularly relevant when the measurement on the inclusion is performed with Raman spectroscopy, that for cubic minerals only allows the volume strain to be determined (Angel et al., 2018) and therefore only allows the application of isotropic geobarometry. The difference between the isotropic and the anisotropic models increases when the symmetry of the inclusion is lower than cubic (e.g. quartz). The discrepancy in general becomes smaller for stiffer hosts, since they can better constrain the inclusion and limit the amount of elastic relaxation. However, there are fundamental assumptions behind our current analysis: the geometry of the system is simple, with a spherical inclusion embedded in an infinite host; the entrapment took place under external hydrostatic conditions; the system did not experience viscous flow. Deviation from any of these assumptions will modify the residual strain/stress field in the inclusion and, if not taken into account appropriately, they would cause larger errors in the back-calculation of the entrapment conditions.

In general, the stress and the strain developed in the inclusion during the exhumation change with different mutual crystallographic orientations between the host and the inclusion. However, we showed that the orientation of a spherical inclusion in a garnet

host does not affect the strain in the inclusion as demonstrated for inclusions with a wide range of stiffness and anisotropy (diamond, quartz and zircon). Therefore, for samples with a simple geometry where the inclusion is almost spherical and isolated within the garnet, and far away from external surfaces, the determination of their relative orientation is not necessary to constrain the entrapment conditions.

We demonstrated the application of this model to systems with simple geometry. It can be also applied to more complex geometries if the three-dimensional model of the sample is available (for example through X-ray micro-tomography). However, the effect of complex geometries on the strain/stress fields should be evaluated on a case-by-case basis and is beyond the scope of this paper.

## Acknowledgements

This project has received funding from the European Research Council (ERC) under the European Union's Horizon 2020 research and innovation programme (grant agreement No 714936 for the project TRUE DEPTHS to M. Alvaro). The authors thank Prof. Matthew Kohn and an anonymous reviewer for their constructive suggestions and comments.

## Appendix A. Supplementary data

Supplementary data to this article can be found online at <https://doi.org/10.1016/j.lithos.2019.105218>.

## References

- Alvaro, M., Mazzucchelli, M.L., Angel, R.J., Murri, M., Campomenosi, N., Scambelluri, M., Nestola, F., Korsakov, A., Tomilenko, A.A., Marone, F., Morana, M., 2020. Fossil subduction recorded by quartz from the coesite stability field. *Geology* 48. <https://doi.org/10.1130/G46617.1>.
- Angel, R.J., Alvaro, M., Gonzalez-Platas, J., 2014a. EosFit7c and a Fortran module (library) for equation of state calculations. *Zeitschrift für Krist. Mater.* 229, 405–419.
- Angel, R.J., Alvaro, M., Miletich, R., Nestola, F., 2017a. A simple and generalised P–T–V EoS for continuous phase transitions, implemented in EosFit and applied to quartz. *Contrib. Mineral. Petrol.* 172, 29. <https://doi.org/10.1007/s00410-017-1349-x>.
- Angel, R.J., Alvaro, M., Nestola, F., Mazzucchelli, M.L., 2015a. Diamond thermoelastic properties and implications for determining the pressure of formation of diamond-inclusion systems. *Russ. Geol. Geophys.* 56 <https://doi.org/10.1016/j.rgg.2015.01.014>.
- Angel, R.J., Jackson, J.M., Reichmann, H.J., Speziale, S., 2009. Elasticity measurements on minerals: a review. *Eur. J. Mineral.* 21, 525–550. <https://doi.org/10.1127/0935-1221/2009/0021-1925>.
- Angel, R.J., Mazzucchelli, M.L., Alvaro, M., Nestola, F., 2017b. EosFit-Pinc: a simple GUI for host-inclusion elastic thermobarometry. *Am. Mineral.* 102, 1957–1960. <https://doi.org/10.2138/am-2017-6190>.
- Angel, R.J., Mazzucchelli, M.L.M.L., Alvaro, M., Nimis, P., Nestola, F., 2014b. Geobarometry from host-inclusion systems: the role of elastic relaxation. *Am. Mineral.* 99, 2146–2149. <https://doi.org/10.2138/am-2014-5047>.
- Angel, R.J., Milani, S., Alvaro, M., Nestola, F., 2016. High-quality structures at high pressure? Insights from inclusions in diamonds. *Z. für Kristallogr. - Cryst. Mater.* 0, 1–8. <https://doi.org/10.1515/zkri-2016-1949>.
- Angel, R.J., Murri, M., Mihailova, B., Alvaro, M., 2018. Stress, strain and Raman shifts. *Zeitschrift für Krist. Mater.* 234, 129–140. <https://doi.org/10.1515/zkri-2018-2112>.
- Angel, R.J., Nimis, P., Mazzucchelli, M.L., Alvaro, M., Nestola, F., 2015b. How large are departures from lithostatic pressure? Constraints from host–inclusion elasticity. *J. Metamorph. Geol.* 33, 801–813. <https://doi.org/10.1111/jmg.12138>.
- Anzolini, C., Nestola, F., Mazzucchelli, M.L., Alvaro, M., Nimis, P., Gianese, A., Morganti, S., Marone, F., Campione, M., Hutchison, M.T., Harris, J.W., 2019. Depth of diamond formation obtained from single periclase inclusions. *Geology* 47, 219–222. <https://doi.org/10.1130/G45605.1>.
- Bonazzi, M., Tumiati, S., Thomas, J., Angel, R., Alvaro, M., n.d. Assessing the Reliability of Elastic Geobarometry Methods. prep.
- Bose, K., Ganguly, J., 1995. Quartz-coesite transition revisited: reversed experimental determination at 500–1200°C and retrieved thermochemical properties. *Am. Mineral.* 80 (3–4), 231–238. <https://doi.org/10.2138/am-1995-3-404>.
- Burnley, P.C., Schmidt, C., 2006. Finite element modeling of elastic volume changes in fluid inclusions: comparison with experiment. *Am. Mineral.* 91, 1807–1814.
- Campomenosi, N., Mazzucchelli, M.L., Mihailova, B., Scambelluri, M., Angel, R.J., Nestola, F., Reali, A., Alvaro, M., 2018. How geometry and anisotropy affect residual strain in host-inclusion systems: coupling experimental and numerical

- approaches. *Am. Mineral.* 103, 2032–2035. <https://doi.org/10.2138/am-2018-6700CCBY>.
- Chiang, C.R., 2017. On Eshelby's tensor in transversely isotropic materials. *Acta Mech.* 228, 1819–1833. <https://doi.org/10.1007/s00707-017-1811-x>.
- Day, H.W., 2012. A revised diamond-graphite transition curve. *Am. Mineral.* 97, 52–62. <https://doi.org/10.2138/am.2011.3763>.
- Enami, M., Nishiyama, T., Mouri, T., 2007. Laser Raman microspectrometry of metamorphic quartz: a simple method for comparison of metamorphic pressures. *Am. Mineral.* 92, 1303–1315. <https://doi.org/10.2138/am.2007.2438>.
- Eshelby, J., 1957. The determination of the elastic field of an ellipsoidal inclusion, and related problems. In: *Proceedings of the Royal Society of London A: Mathematical, Physical and Engineering Sciences*. The Royal Society, pp. 376–396.
- Guiraud, M., Powell, R., 2006. P–V–T relationships and mineral equilibria in inclusions in minerals. *Earth Planet. Sci. Lett.* 244, 683–694. <https://doi.org/10.1016/j.epsl.2006.02.021>.
- Hughes, T.J.R., 2012. *The Finite Element Method: Linear Static and Dynamic Finite Element Analysis*. Courier Corporation.
- Isaak, D.G., Anderson, O.L., Oda, H., 1992. High-temperature thermal expansion and elasticity of calcium-rich garnets. *Phys. Chem. Miner.* 19, 106–120. <https://doi.org/10.1007/bf00198608>.
- Karato, S., Wang, Z., Liu, B., Fujino, K., 1995. Plastic deformation of garnets: systematics and implications for the rheology of the mantle transition zone. *Earth Planet. Sci. Lett.* 130, 13–30. [https://doi.org/10.1016/0012-821X\(94\)00255-W](https://doi.org/10.1016/0012-821X(94)00255-W).
- Lakshtanov, D.L., Sinogeikin, S.V., Bass, J.D., 2007. High-temperature phase transitions and elasticity of silica polymorphs. *Phys. Chem. Miner.* 34, 11–22. <https://doi.org/10.1007/s00269-006-0113-y>.
- Mazzucchelli, M.L.L., Burnley, P., Angel, R.J.J., Morganti, S., Domeneghetti, M.C.C., Nestola, F., Alvaro, M., 2018. Elastic geothermobarometry: corrections for the geometry of the host-inclusion system. *Geology* 46, 231–234. <https://doi.org/10.1130/G39807.1>.
- Milani, S., Angel, R.J., Scandolo, L., Mazzucchelli, M.L., Ballaran, T.B., Klemme, S., Domeneghetti, M.C., Miletich, R., Scheidl, K.S., Derzsi, M., Tokár, K., Prencipe, M., Alvaro, M., Nestola, F., 2017. Thermo-elastic behavior of grossular garnet at high pressures and temperatures. *Am. Mineral.* 102, 851–859. <https://doi.org/10.2138/am-2017-5855>.
- Milani, S., Nestola, F., Alvaro, M., Pasqual, D., Mazzucchelli, M.L., Domeneghetti, M.C., Geiger, C.A., 2015. Diamond–garnet geobarometry: the role of garnet compressibility and expansivity. *Lithos* 227, 140–147. <https://doi.org/10.1016/j.lithos.2015.03.017>.
- Murri, M., Mazzucchelli, M.L., Campomenosi, N., Korsakov, A.V., Prencipe, M., Mihailova, B.D., Scambelluri, M., John, A.R., Matteo, A., Angel, R.J., Alvaro, M., 2018. Raman elastic geobarometry for anisotropic mineral inclusions. *Am. Mineral.* 103, 1869–1872. <https://doi.org/10.2138/am-2018-6625CCBY>.
- Nye, J.F., 1985. *Physical Properties of Crystals: Their Representation by Tensors and Matrices*. Oxford University Press, Oxford.
- Özkan, H., Cartz, L., Jamieson, J.C., 1974. Elastic constants of nonmetamict zirconium silicate. *J. Appl. Phys.* 45, 556–562. <https://doi.org/10.1063/1.1663283>.
- Sinogeikin, S.V., Bass, J.D., 2002. Elasticity of pyrope and majorite-pyrope solid solutions to high temperatures. *Earth Planet. Sci. Lett.* 203, 549–555.
- Thomas, J.B., Spear, F.S., 2018. Experimental study of quartz inclusions in garnet at pressures up to 3.0 GPa: evaluating validity of the quartz-in-garnet inclusion elastic thermobarometer. *Contrib. Mineral. Petrol.* 173, 1–14.
- Voigt, W., 1910. *Lehrbuch der Kristallphysik. Kristallographie*. Teubner, Leipzig.
- Wang, J., Mao, Z., Jiang, F., Duffy, T.S., 2015. Elasticity of single-crystal quartz to 10 GPa. *Phys. Chem. Miner.* 42, 203–212. <https://doi.org/10.1007/s00269-014-0711-z>.
- Zaffiro, G., 2019. *Elastic Geobarometry: In-Situ Single-Crystal X-Ray Diffraction Measurements of Inclusions Trapped in Host Minerals to Determine the Entrapment Conditions*. University of Pavia, Pavia.
- Zhang, Y., 1998. Mechanical and phase equilibria in inclusion-host systems. *Earth Planet. Sci. Lett.* 157, 209–222.
- Zhong, X., Moulas, E., Tajčmanová, L., 2018. Tiny timekeepers witnessing high-rate exhumation processes. *Sci. Rep.* 8, 1–9. <https://doi.org/10.1038/s41598-018-20291-7>.
- Zouboulis, E., Grimsditch, M., Ramdas, a., Rodriguez, S., 1998. Temperature dependence of the elastic moduli of diamond: a Brillouin-scattering study. *Phys. Rev. B* 57, 2889–2896. <https://doi.org/10.1103/PhysRevB.57.2889>.